March 2008

# Search for Coincidence Events in LIGO and GEO600 Data

Olga Petrovna Petrova
*Worcester Polytechnic Institute*

# Contents

# List of Figures

# List of Tables



:

# Part I

# Gravitational Waves

# Chapter 1

# Introduction to Gravity Waves

## 1.1 Gravity Waves - Ripples in Spacetime

In *The Search for Gravity Waves* ([5]), Davies introduces a rather simple way to think about spacetime. First, let us consider tidal gravity acting on a cube of matter, which we allow to fall freely in a non-uniform gravitational field. Since the base of the block is closer to Earth, the gravitational force acting on it will be stronger than that acting on its top. Therefore, tidal gravity will try to stretch it vertically. This example can be extended to show that since gravity deforms all freely-falling objects in identical ways, the effect can be viewed as geometrical, rather than mechanical. This was the approach taken by Albert Einstein when he proposed gravity to be a manifestation of spacetime geometry. A distortion from flat geometry could cause objects to drift relative to each other, just as though tidal forces were acting [5]. Without going into the details of Einsteins theory of General relativity, we can say that he did find that wavelike solutions to his gravitational field equation exist.

Davies further shows why gravitational dipoles cannot generate gravity waves [5]. First, he considers two equal masses joined by a spring (Fig. 1a). As the spring contracts the leftward motion of one mass opposes the rightward motion of the other. Thus, the center of mass of the system does not move and the dipole does not oscillate. In the second case, Davies considers two unequal masses, also joined by a spring (Fig. 1b). When the spring

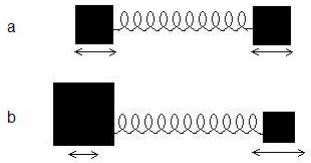


Figure 1.1: Gravitational dipoles do not emit gravity waves (GW)

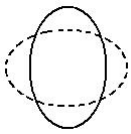

Figure 1.2: Effect of GW (broken lines represent the distortion half a cycle later) on a mass

contracts it pulls the light particle to the left, but by Newtons 3rd law the remote end pulls the heavy mass to the right. Since the heavy mass has a much greater gravitational action, it cancels the gravitational dipole motion due to the light mass. The center of mass still does not oscillate. It turns out that if we look at these systems as quadruples (where each individual mass acts as an oscillating dipole), they do in fact emit gravitational radiation. Because of the time required for the gravitational disturbance from one oscillating dipole to the other to propagate across the length of the spring, the two disturbances are slightly out of phase and dont cancel.

In order to show the effect of gravitational waves on the objects they are passing through, Davies uses a flexible ring placed perpendicular to the wave-propagation vector as an example. During the first half-cycle the distortion is one direction, then in the second half-cycle it is in perpendicular direction. This illustrates waves representation as the passage of a pulse of tidal gravity.

## 1.2 Interaction with Matter

Let's consider a transverse-traceless gauge, in which the spatial components of the coordinate system are fixed to the geodesics of freely falling masses

[3]. Let $T$ be the time it takes a photon to travel between two freely falling masses, as measured by an observer fixed to one of the masses. The invariant interval $s$ has to be zero for a photon. For masses separated in $x$, consider the relation

$dt^2 = (1 + h_+)dx^2$.

Since the end points of the path are fixed, the round trip time travel of the photon is given by

$T = 2\int_0^L (1 + h_+)^{1/2} dx$
where $L$ is the x-directed separation of the two masses in the absence of a gravitational wave. Assuming $h_+ << 1$ and approximately constant over $T$, T can be approximated as

$T \approx 2(1 + \frac{h_+}{2})L$
where $h_+$ is a measure of the fractional change in proper distance between two free masses, which is referred to as a gravitational-wave strain.

## 1.3 Sources of Gravitational Waves

From the discussion above it follows that what is needed for emitting gravitational radiation is a changing quadruple of mass. However, since the proposed effect of gravitational waves is so weak, at this point we can only hope to detect gravitational radiation emitted by enormous astronomical sources, such as stars orbiting each other, stars formation and explosion, disruption of spacetime caused by black holes, etc.

Some of the more plausible astrophysical sources of GW include the coalescence of compact objects such as binary neutron stars and binary black holes, core collapse supernovae of massive stars, ring down oscillations of perturbed black holes, instabilities of rotating neutron stars, and gamma ray bursts [3]. All these are sources of transient gravitational radiation. Sources of continuous gravitational radiation include pulsars, and gravitational waves from the very early universe.

The product of the transient sources of gravitational radiation are the gravitational-wave bursts, the focus of this project. A gravitational-wave

burst is defined as "time-varying strain in space that is sufficiently well localized in time that its time-domain amplitude is square integrable." [3] It is assumed that such bursts are shorter than one second, which conveniently constrains the space of possible signals, while still encompassing the majority of the potentially detectable transient astrophysical sources that fall within the sensitive frequency band of ground based interferometric detectors.

# Chapter 2

# Detection of Gravitational Waves

## 2.1 History of the GW Detection

### 2.1.1 Indirect Evidence of Gravitational Waves

The 1993 Nobel Prize in Physics went to Russell Alan Hulse and Joseph Hooton Taylor for the discovery of PSR B1913+16, a pulsar in a binary star system. Since its discovery, the two stars have been detected to spiral toward each other in precise agreement with the energy loss due to gravitational radiation emission predicted by General Relativity[1].

Although there is strong indirect evidence of the existence of gravitational radiation, gravitational waves have not yet been observed. Not only would such an observation provide strong experimental proof for the General Relativity, but it could also dramatically expand our knowledge of the cosmos [3]. Unlike electromagnetic radiation, gravitational waves are not easily absorbed or scattered by matter, and thus permit observation of regions that are currently inaccessible due to photon and neutrino scattering such as core collapse supernovae or the coalescence of binary compact objects such as neutron stars and black holes. The nature of gravitational radiation also

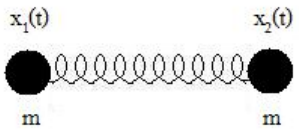


Figure 2.1: Idealized Resonant Mass Detector

suggests the possibility of discovering previously unknown phenomena.

### 2.1.2 Resonant Mass Detectors

An idealized resonant mass detector can be pictured as two point masses $m$ that are connected by a massless spring with spring constant $k$, damping constant $\nu$, and unstretched length $l_0$ [8]. (See Figure 2.1) The system is one dimensional and the two masses have coordinate positions $x_1$ and $x_2$ respectively. The equations the masses would obey in flat space-time are:

$$mx_{1,00} = -k(x_1 - x_2 + l_0) - \nu(x_1 - x_2)_{,0}$$

and

$$mx_{2,00} = -k(x_2 - x_1 + l_0) - \nu(x_2 - x_1)_{,0}.$$

By defining $\xi = x_2 - x_1 - l_0$, $\omega_0^2 = 2k/m$, and $\gamma = \nu/m$ we can get the damped harmonic oscillator equation:

$$\xi_{,00} + 2\gamma_{,0} + \omega_0^2\xi = 0.$$

A point $x_1$ in a local inertial frame which is at rest before the gravitational wave passes remains at rest afterwords. Let its coordinates be $\{x^{\alpha'}\}$ and the only motions in the system are those produced by the wave. Then we can use Newton's equations for the masses in the local inertial frame:

$$mx^{j'}_{,0'0'} = F^{j'}$$

where $\{F^{j'}\}$ are the components of any nongravitational forces acting on the masses, i.e. those due to the spring. The proper length of the spring is then

given by:

$l(t) = \int_{x_1(t)}^{x_2(t)} (1 + h_+(t))^{1/2} dt.$

We can also redefine $\xi$ as $\xi = l - l_0$ and after some manipulations obtain the expression which is correct to first order in $h_+$:

$\xi_{,00} + 2\gamma_{,0} + \omega_0^2 \xi = \frac{1}{2} l_0 h_{+,00}.$

This equation, governing the response of the resonant detector to the gravitational wave, has a form of a forced, damped harmonic oscillator. A detector of this sort can be used for sources of gravitational radiation of a fixed frequency (e.g. pulsars or close binary stars). When aiming to detect a source whose frequency is known, we can adjust $\omega_0$ to that frequency for maximum response [8].

### 2.1.3 Interferometric Detectors

In the case of an interferometric detector, the gravitational wave strain is given by [3]

$h(t) = F_+ h_+(t) + F_x h_x(t).$

where coefficients $F_+$ and $F_x$ are dependent on the polarization of the wave and position of the GW source with respect to the detector.

Figure 2.2 shows a simplified schematic of the LIGO detectors [3], which illustrates how most modern interferometric detectors work. There is a number of interferometric detectors currently operating around the world. In combination with resonant mass detectors, they provide the means for strong verification tests for candidate events. The focus of this project was on the three LIGO detectors (USA) and the GEO600 detector in Germany, which are described in detail in the next two sections.

### 2.1.4 Future of Gravitational Wave Detection

The advantages of a space-based interferometer over a ground-based one include a much larger size of the former, as well as the obvious absence of terrestrial noise sources. These would allow a space-based detector to search for gravitational waves at low frequencies that are unaccessible to

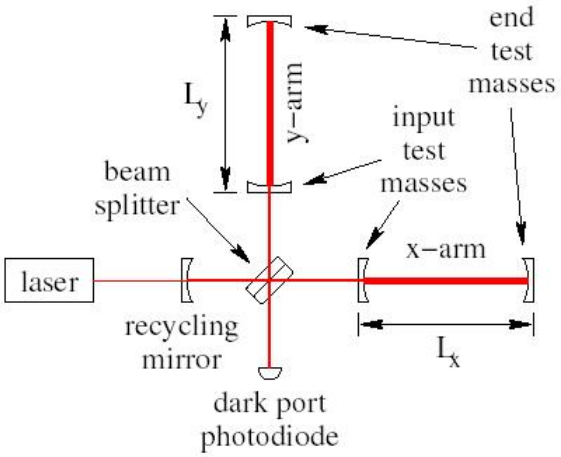


Figure 2.2: "The detectors consist of a modified Michelson interferometer with Fabry-Perot cavity arms in order to increase the differential phase delay due to incident gravitational waves. The detector is nominally operated such that the optical power at the anti-symmetric photodiode is minimized. At this operating point, the entire interferometer behaves like a single mirror and a recycling mirror allows for greater circulating light power in the detector."[3]

ground-based detectors. Such an interferometer, called Laser Interferometer Space Antenna (LISA), is currently being developed as a joint ESA/NASA mission. Upon completion, LISA will be able to probe gravitational-waves in the frequency band from $10^{-4}$ to $10^{-1}$ Hz.

## 2.2 LIGO

Laser Interferometer Gravitational Wave Observatory (LIGO) consists of three interferometric detectors[3]. Two of them, with 2 and 4 km arm lengths, are located in Hanford, Washington. These are co-aligned, and therefore the detected strains due to a gravitational wave are expected to vary by a factor

of two due to the difference in arm lengths. The third LIGO interferometer also has 4 km long arms and is located in Livingston, Louisiana. Except for slightly different tangent planes due to the curvature of the Earth, the two sites are approximately aligned to respond to the same gravitational-wave polarization.

The LIGO detectors are Michelson interferometers illuminated by 10 Watt solid state Nd:YAG lasers with a wavelength of 1064 nm. In order to increase the accumulated phase delay resulting from incident gravitational waves, the interferometer arms are comprised of Fabry-Perot resonant cavities such that the approximate light storage time in the arms is on the order of 1 millisecond. In order to isolate the LIGO detectors from terrestrial noise sources, the interferometers are maintained in a vacuum of between $10^{-8}$ $10^{-9}$ mbar. The optical tables within the vacuum envelope are then isolated from ground vibrations by 3 alternating stacks of stainless steel and dissipative bronze springs. The test masses are further isolated by pendular suspensions such that they behave like free masses for excitations above their resonant frequency of approximately 1 Hz.

## 2.3 GEO600

GEO600 is another ground-based laser interferometer, with 600 m long arms, which uses the same type of laser as the LIGO detectors do. It is located near Hannover, Germany. Its sensitivity for gravitational wave bursts reaches $h \approx 10^{-20}...10^{-21}$, with a frequency range of 50 Hz to 1.5 kHz.

# Part II

# Data Analysis

# Chapter 3

# KleineWelle Analysis Method

There are different ways to identify bursts of gravitational radiation. Virtually all of the search algorithms "operate by linearly projecting the data under test onto a suitably chosen measurement basis"[3].

The KleineWelle algorithm is a wavelet-based multiresolution method used to find and analyze transients in an input timeseries. The wavelet transform was chosen due to its time-frequency localization, achieved by using time windows. These windows allow the wavelet transform to "zoom-in" and "zoom-out" as needed, as opposed to the Fourier transform, which represents the signal over its entire spectrum. This feature is especially useful when analyzing signals with discontinuities and sharp spikes. The general form of the continuous wavelet transform (WT) of a signal $f(t)$ is given by the following integral:

$$W_\Psi f(\alpha, b) = |\alpha|^{-1/2} \int f(t)\overline{\Psi(\tfrac{t-b}{\alpha})}dt$$

where $\alpha$ and b are real and $\Psi(t)$ is assumed to be a complex function satisfying the condition $\int \Psi(t)dt = 0$.

The so-called wavelets functions of the form $\Psi^{\alpha,b} = |\alpha|^{-1/2} \Psi(\frac{t-b}{\alpha})$ are obtained by dilations (by $\alpha$) and translations (by $b$) of the mother wavelet $\Psi$ (in other words, parameter b shifts the center of $\Psi$, while $\alpha$ compresses or stretches it). It can be shown that the inverse wavelet transform is given by

$$f = C_\Psi^{-1} \int \int \tfrac{d\alpha db}{\alpha^2} W_\Psi f(\alpha, b)\Psi^(\alpha, b)$$

where $C_\Psi^{-1} = 2\pi \int d\omega \frac{\left|\hat{\Psi}(\omega)\right|^2}{|\omega|}$

In both the continuous and discrete WT, the analyzing functions $\Psi$ adjust their resolution in order to match their scale (frequency): small values of $\alpha$ yield high-frequency spectral information of the signal and in order to give better accuracy the resolution (time-interval) is finer; on the other hand using large values of $\alpha$ allows us to see gross features. This is what gives WT its unique time-frequency localization property.

When analyzing discrete data, one can use the dyadic wavelet transform in order to calculate wavelet coefficients over scales that vary as powers of two more efficiently [2]. The detail coefficients, $D_j$, and the approximation coefficients, $A_j$ are defined at each level j of the decomposition and are given by

$$D_j = \hat{H}(A_{j-1}) \text{ and } A_j = \hat{L}(A_{j-1}$$

where $\hat{H}$ is a high pass filter, $\hat{L}$ a low pass filter, and $A_0$ refers to the original time series.

Prior to passing the data to the dyadic wavelet transform, KleineWelle "whitens" it by using linear predictive filtering [2]. For a sufficiently large $j$, the wavelet coefficients $D_j$ within the scale $j$ approach a zero-mean Gaussian distribution with standard deviation $\sigma_j$. The sequence of squared normalized coefficients, or normalized pixel energies at scale $2^j$ is defined as:

$$E_j = D_j^2/\sigma_j^2,$$

In order to identify statistical outliers, a threshold on the energy of individual pixels, $\epsilon_{ij} \in E_j$, is applied. Nearby pixels are clustered for easier detection of bursts which deviate from the dyadic wavelet tiling of the time-frequency plane. For a randomly selected cluster C of N pixels, the total normalized cluster energy is

$$E_C = \sum_{(i,j)\in C} \epsilon_{ij}.$$

The significance of this cluster of pixels is defined by,

$$S = -\ln \int_{E_C}^{\infty} X_N^2(E) dE.$$

The significance is a function of cluster energy $E_C$ and the number of pixels in the cluster N, which makes it possible to select a threshold significance to achieve a desired white noise false event rate.

The wavelet coefficients that pass a certain amplitude threshold are stored as pixels in a vector of Element structures, each of which contains information about the pixels time and scale, as well as its unnormalized and normalized energy.

The pixels are run through a recursive clustering algorithm which takes nearby pixels and clusters them into a single cluster represented by an Event structure. Each cluster is represented by an Event structure, and contains derived quantities such as the absolute start and end times of the event, the energy weighted central time, the energy weighted central scale, and the cluster significance. Clusters which pass the significance threshold are output in a standardized multicolumn ASCII format. The current list of columns is,

- start time
- end time
- peak time
- central frequency
- unnormalized energy
- normalized energy
- number of pixels
- significance

These eight columns constitute trigger files that are used for analyzing data from single IFOs, which will be described in more detail in Section 5.1.

# Chapter 4

# The Data

## 4.1 Livetime Analyzed

The data analyzed was collected in coincidence by GEO600 and only one of the three LIGO interferometers (i.e., only one LIGO IFO was collecting data at any given time) in the first year of the S5 science run, that is the time period between Nov 04 2005 15:59:47 UTC and Nov 04 2006 15:59:46 UTC. In addition to the data quality flags, which are described below, all segments less than 600 seconds long were rejected. As a result, the three combinations of detectors (G1H1, G1H2, and G1L1) were analyzed whose total and effective (i.e., left after rejecting segments less than 600 seconds) livetimes are summarized in Table 4.1.

| | total (sec) | effective (sec) |
|---|---|---|
| G1H1 | 163641 | 121483 |
| G1H2 | 373144 | 315922 |
| G1L1 | 432732 | 351368 |

Table 4.1: Total and Effective Livetimes for G1H1, G1H2, and G1L1

## 4.2 Data Quality Flags

As briefly mentioned in Chapter 3, triggers are the candidate GW events detected by interferometers. Sections of bad data due to poor interferometer performance or environmental disturbance are excluded from the analysis. When these sections are identified, a data quality flag is produced. When triggers are in coincidence with short duration glitching in interferometer or environmental channels, vetoes are developed [4].

In this analysis, the so-called category I and II data quality flags were used, namely:

- AS_TRIGGER: under certain conditions of saturation, the interferometer's output beam to the antisymmetric port's four photodiodes is temporarily diverted to a fifth photodiode, to avoid lock loss and resulting prolonged downtime. The triggering of this diverted light automatically takes the interferometer out of science mode.

- INJECTION: hardware signal injections are flagged automatically in the publishing of science segments.

- INVALID_DARMERR: is set whenever the data-valid flag is found to be invalid for the gravitational wave data channel.

- MISSING_RDS_C02_LX: the program that generates calibrated strain data (h(t)), uses finite-impulse-response filters that require a settling time of up to 8 seconds (H2 and L1) or 16 seconds (H1), leading to short gaps at the starts and stops of many data segments (the filters run both forward and backward). This data quality flag is generated due to the missing h(t) segments in S5 RDS frames where most of the gaps come from the filtering effects.

- MISSING_RDS_LEVEL_1: both level 1 and level 3 flags correspond to missing reduced data sets

- MISSING_RDS_LEVEL_3

- OUT_OF_LOCK: the published science segments are derived from the slow EPICS state vector channel which is delayed by 1-2 seconds in responding to lock loss. As a result, many science segments include 1-2 seconds of unlocked data at their ends.

- PRE_LOCKLOSS_30_SEC: it has been found that the period immediately preceding lock loss is marked by increased noise, particularly glitchiness.
- CORRUPTED_RDS_C02_LX: marks corrupted, unrecoverable strain data.
- CALIB_DROPOUT_1SAMPLE: the next five data quality flags are due to the fact that arbitrary waveform generator (awg) used for injecting calibration lines and astrophysical signals occasionally malfunctions.
- CALIB_DROPOUT_1SEC
- CALIB_DROPOUT_AWG_STUCK
- CALIB_DROPOUT_BN
- CALIB_GLITCH_ZG
- SEVERE_LSC_OVERFLOW
- ASC_OVERFLOW
- ASI_CORR_OVERFLOW
- CALIB_BAD_COEFFS_60: When the gravitational wave servo gain fluctuates a large amount (e.g., via uncompensated optical gain loss from mirror wobble), the servo can become less stable, leading to increased noise, including saturation.
- MASTER_OVERFLOW_ASC: the next two flags keep track of overflows detected in ADC's and in calculations and increments various "master counters" of such overflows
- MASTER_OVERFLOW_SUS_RM
- POWMAG: corresponds to a list of glitches on multiple magnetometers at Hanford or Livingston. These glitches are sometimes associated with glitches in the gravitational wave channel. Many coincide with disturbances on the power mains [7]

# Chapter 5

# Method

## 5.1 Analyzing Data from a Single Interferometer

The code that processes triggers for single IFOs needs the following input files: segments, triggers, vetoes, and a configuration file (the last two are optional).

One of the output files that is generated is *strigs.txt*, which contains the following fields:

- trigger number (obsolete)
- trigger start time (GPS with start of day/S5 subtracted)
- ifo (obsolete)
- trigger significance
- trigger number of pixels
- trigger central frequency
- trigger unnormalized energy

- trigger duration
- trigger normalized energy
- segment start (GPS with start of day/S5 subtracted)
- segment duration
- segmener number
- number of vetoes coinciding with trigger
- time difference between start time of the trigger and start time of the nearest veto (-1 if no vetoes available)
- veto number (obsolete)
- pointer to the veto array (valid if >= 0)
- veto time if vetoed, otherwise -1
- veto duration if vetoed, otherwise -1
- veto significance if vetoed, otherwise -1
- veto CENTRAL frequency if vetoed, otherwise -1

If a positive time window for clustering was provided by the user, single events that overlaped within that window were clustered into one event and *ctrigs.txt* file was generated. The structure of this file is similar to that of *strigs.txt*, but has some extra fields, such as multiplicity - number of single events in a cluster.

*Vsum.txt* contains a summary (which includes number of events, rate of occurrence, start times of the first and last events) of single events, vetoes, clustered events for each segment, as well as statistics for total livetime analyzed. The latter includes the mean value, RMS, and standard deviation for the event rates, livetime lost due to vetoes, and average veto efficiency.

If a veto file was provided, vetoes are time-shifted with respect to triggers, and a non-empty *vsum-shifts.tx*t file is generated, that contains information about veto usage and veto efficiency for each time shift for both single and clustered events. For the purposes of this project, this functionality was not used.

## 5.2 Searching for Events Coincident in Two Detectors

### 5.2.1 The Code

The program that finds coincidences between two detectors takes in two *strigs.txt* files produced by the code that processes the data from a single interferometer (described above). The user specifies the following parameters: the minimum significance (amplitude) of the events to be read from the input files, the coincidence window in seconds for finding events that overlap for the two detectors, and $\delta T$ - the time in seconds by which the time series of one detector is shifted with respect to the other one. There is a total of 101 such time-shifts - 50 backward, 50 forward, as well as the zero time shift which is just the original time series.

The ouput consists of three files: *tlags-evnt.txt*, *tlags-cnts.txt* and *tlags-cf.txt*.

*Tlags-cnts.txt* has the following 5 columns:

- number of the time shift: goes from -50 to 50
- time shift of the first IFO in seconds: equal to $\delta T$ times the value of the first column
- time shift of the second IFO in seconds: equal to zero
- number of coincidences
- total livetime, in seconds

In addition to these five columns, *tlags-evnt.txt* lists the start time and the duration of each coinciding event, and *tlags-cf.txt* lists the central frequencies of the two events detected by the two detectors corresponding to each coincidence. The last lines of *tlags-cnts.txt* and *tlags-evnt.txt* list the event rate (the rate of coincidences for zero time shift) and the background rate (the average rate for non zero time shifted data).

### 5.2.2 Poisson Process

The events detected by two interferometers at the same time can be viewed as a Poisson process. A Poisson process is a stochastic process used for modeling random events that occur to a large extent independently of one another. The Poisson process is a collection $N(t) : t \geq 0$ of random variables, where N(t) is the number of events that have occurred up to time t (starting from time 0). The number of events between time a and time b is given as N(b) - N(a) and has a Poisson distribution.

We can derive the formula for the Poisson distribution from the binomial distribution for the probability of $n$ events out of $N$ attempts where $p$ is the probability of the event for each attempt [6]:

$P(n) = \frac{N!}{n!(N-n)!} p^n (1-p)^{N-n}$.

Next, we can use Stirling's approximation:

$\ln \frac{N!}{(N-n)!} = \ln N! - ln(N-n)!$
$\approx N \ln N - (N-n) \ln(N-n)$
$\approx N \ln N - (N-n) \ln N$
$= N \ln N - N \ln N + n \ln N$
$= n \ln N$

from which we can obtain the relationship

$\frac{N!}{(N-n)!} \approx e^{n \ln N} = N^n$.

For $p << 1$ we can approximate the binomial distribution formula to get the expression for Poisson distribution:

$P(n) = \frac{(Np)^n}{n!} e^{-pN}$.

# Chapter 6

# Results and Discussion

## 6.1 Coincidence Analysis for Single Events

In order to calculate the accidental coincidence rate for two IFOs, the events detected by one of the IFOs were time-shifted by 5 seconds with respect to events detected by the other IFO. A total of 50 backward and 50 forward time shifts were performed for each of the three combinations. The coincidence rates for two significance thresholds (10 and 35) are summarized in Tables 6.1 and 6.2. A coincidence window equal to 0.05 seconds was used.[1]

Figures 6.1 and 6.2 are plots of G1H1 coincidence rates for events louder than 10 and 35 respectively as functions of time shift, where $\delta T = 0$ corresponds to non-shifted data.

[1]Since gravitational waves are expected to travel at the speed of light, the interval between event triggers in the different detectors should be the time light takes to travel between the detectors plus the uncertainty due to our trigger generation mechanisms. For GEO600 and LIGO interferometers this time was approximated as 0.025 seconds. The coincidence window used was taken to be two times that value in order to take into account experimental error due to response of the instruments and timing uncertainty of the search methods.

| | background coincidence rate, Hz | actual coincidence rate, Hz |
|---|---|---|
| G1H1 | .0576585 | .0600577 |
| G1H2 | .0279868 | .0299921 |
| G1L1 | .0332142 | .0359310 |

Table 6.1: Background (accidental) and actual (non time-shifted) coincidence rates for G1H1, G1H2, and G1L1 for events with significance 10 and louder

| | background coincidence rate, Hz | actual coincidence rate, Hz |
|---|---|---|
| G1H1 | 5.93144e-05 | 7.40844e-05 |
| G1H2 | 1.35136e-05 | 1.27708e-05 |
| G1L1 | 1.82959e-05 | 3.69983e-05 |

Table 6.2: Background (accidental) and actual (non time-shifted) coincidence rates for G1H1, G1H2, and G1L1 for events with significance 35 and louder

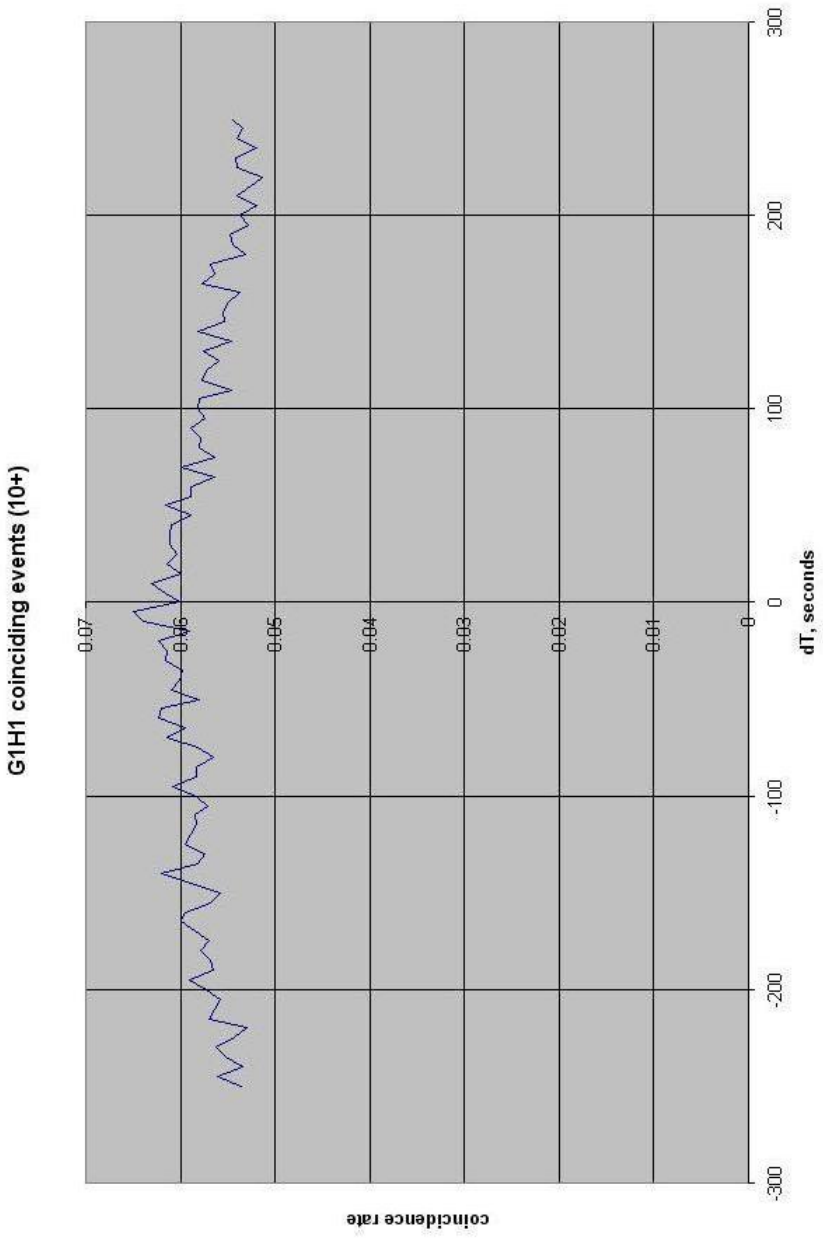


Figure 6.1: Rate of G1H1 coincidences louder than 10 vs. time shift

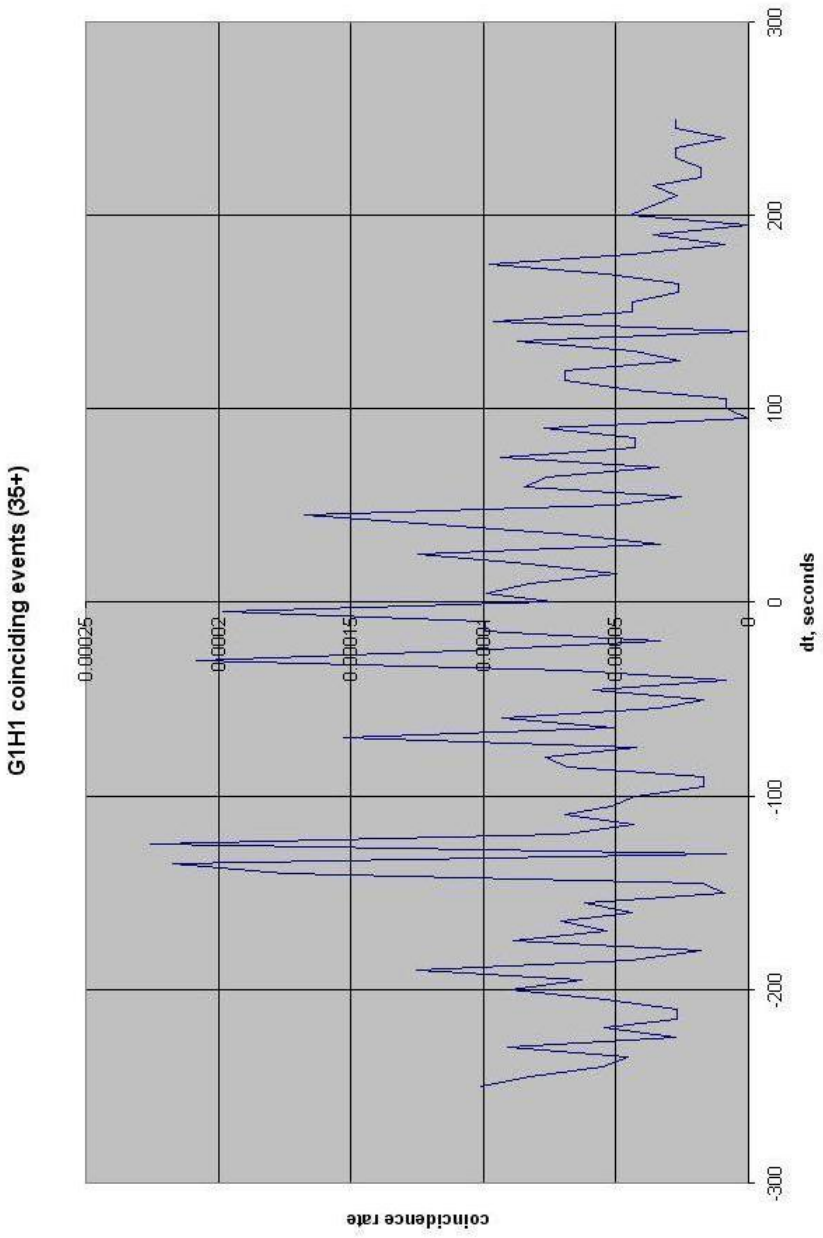


Figure 6.2: Rate of G1H1 coincidences louder than 35 vs. time shift

Coinciding individual events detected by separate IFOs are expected to have nearly equal values of central frequency if they were to correspond to a gravitational wave event. Figures 6.3 and 6.4 provide histograms of central frequencies of coinciding G1 and H1 events for real as well as time shifted data (significance thresholds are set to 10 and 35).

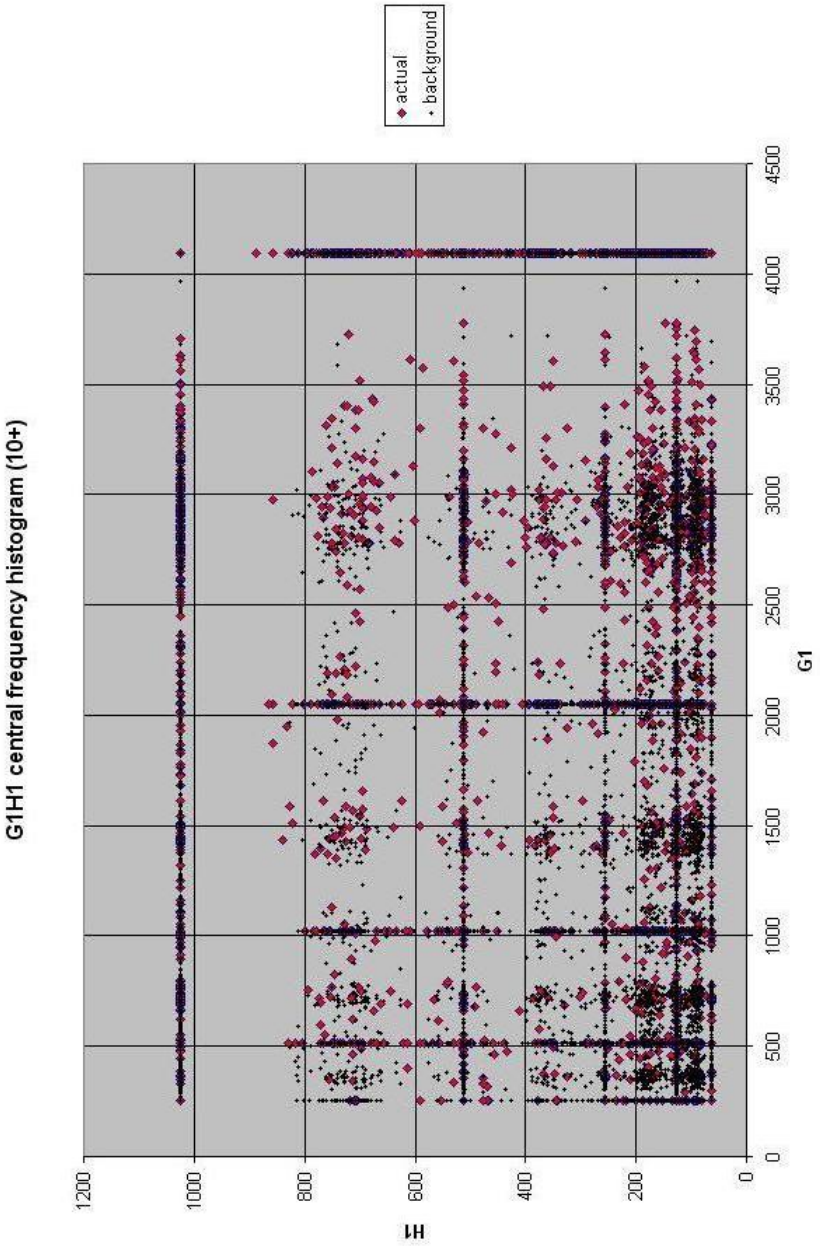


Figure 6.3: Central frequencies of accidental and actual G1H1 coincidences louder than 10

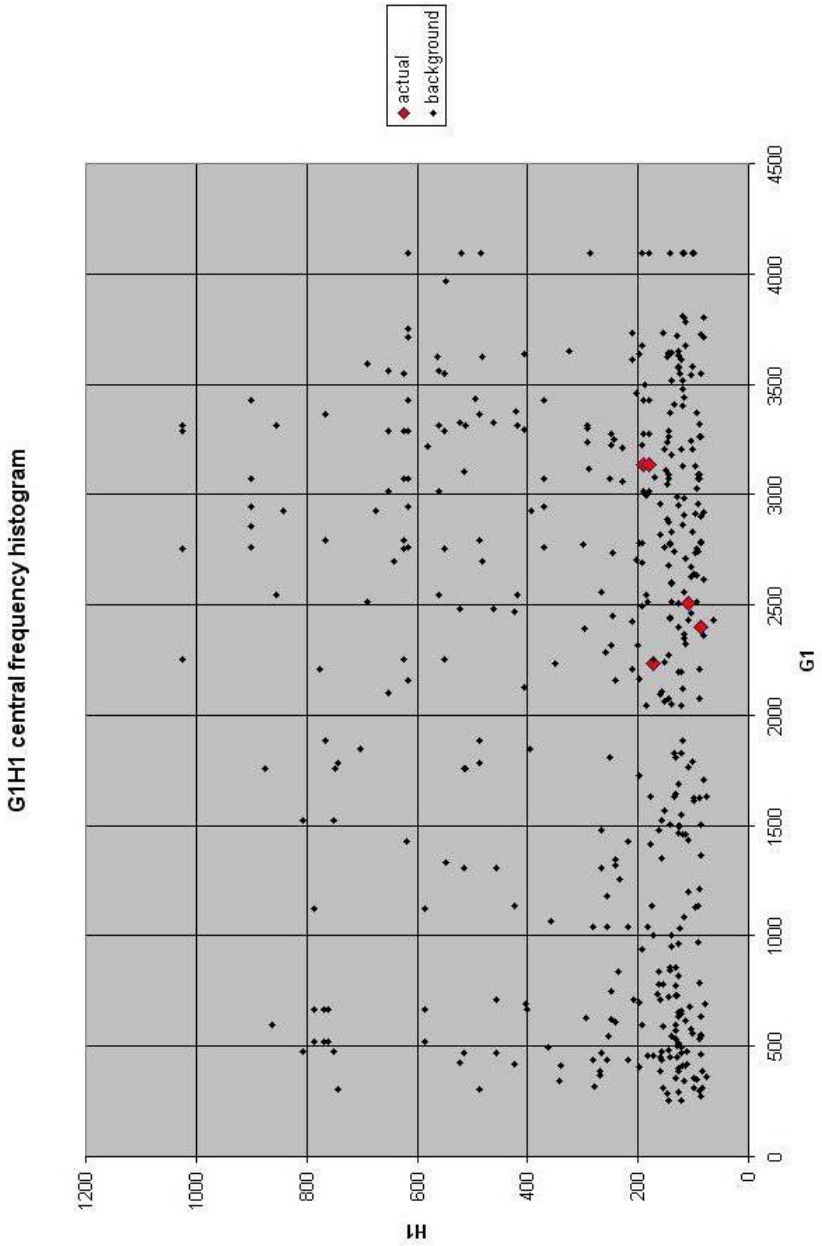


Figure 6.4: Central frequencies of accidental and actual G1H1 coincidences louder than 35

Similarly, Figures 6.6 - 6.12 show the same information about G1H2 and G1L1 coincidences.

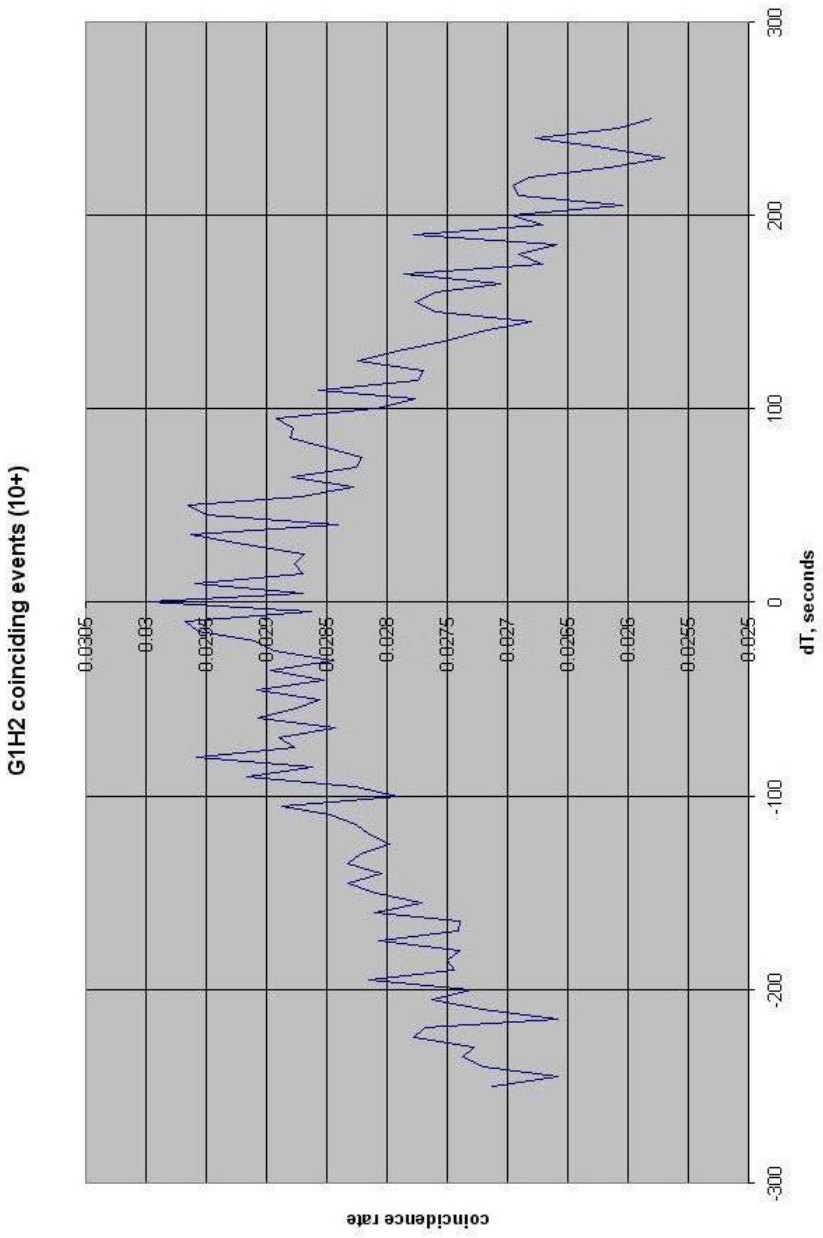


Figure 6.5: Rate of G1H2 coincidences louder than 10 vs. time shift

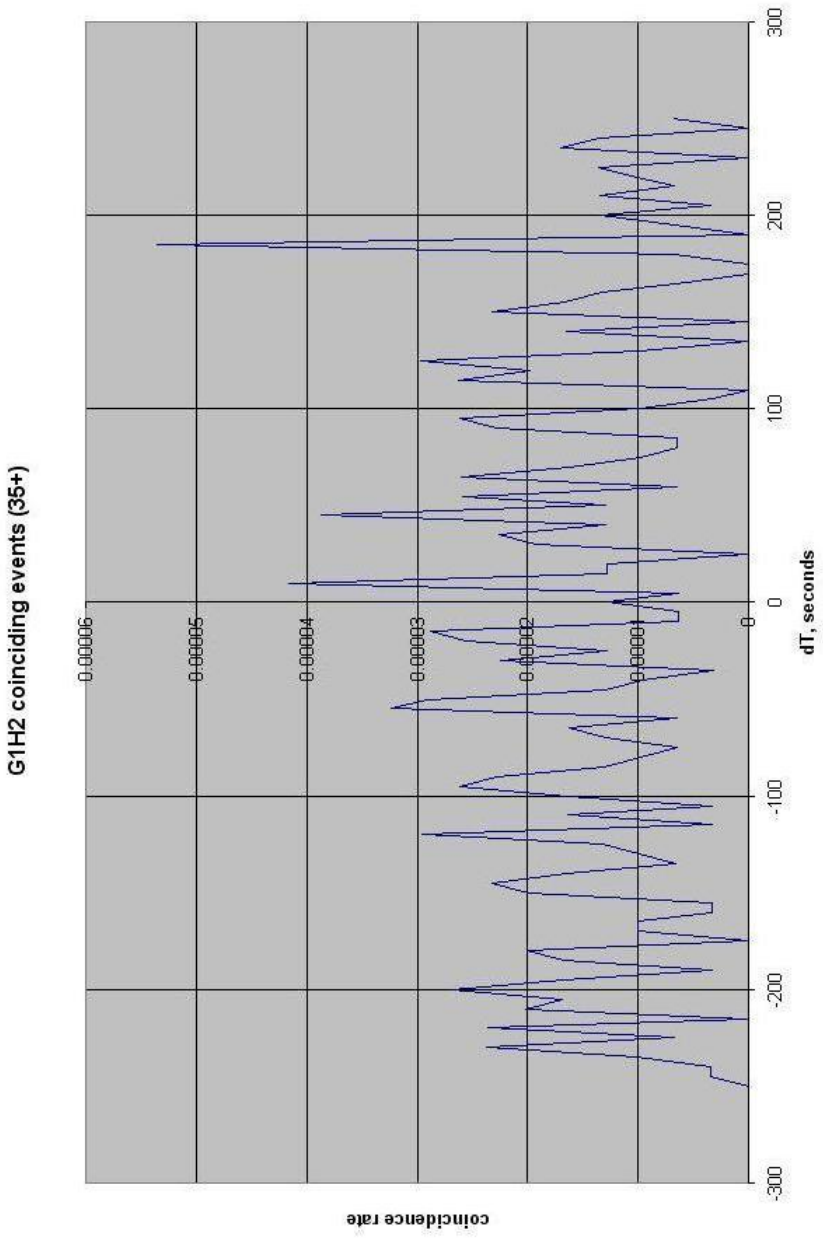


Figure 6.6: Rate of G1H2 coincidences louder than 35 vs. time shift

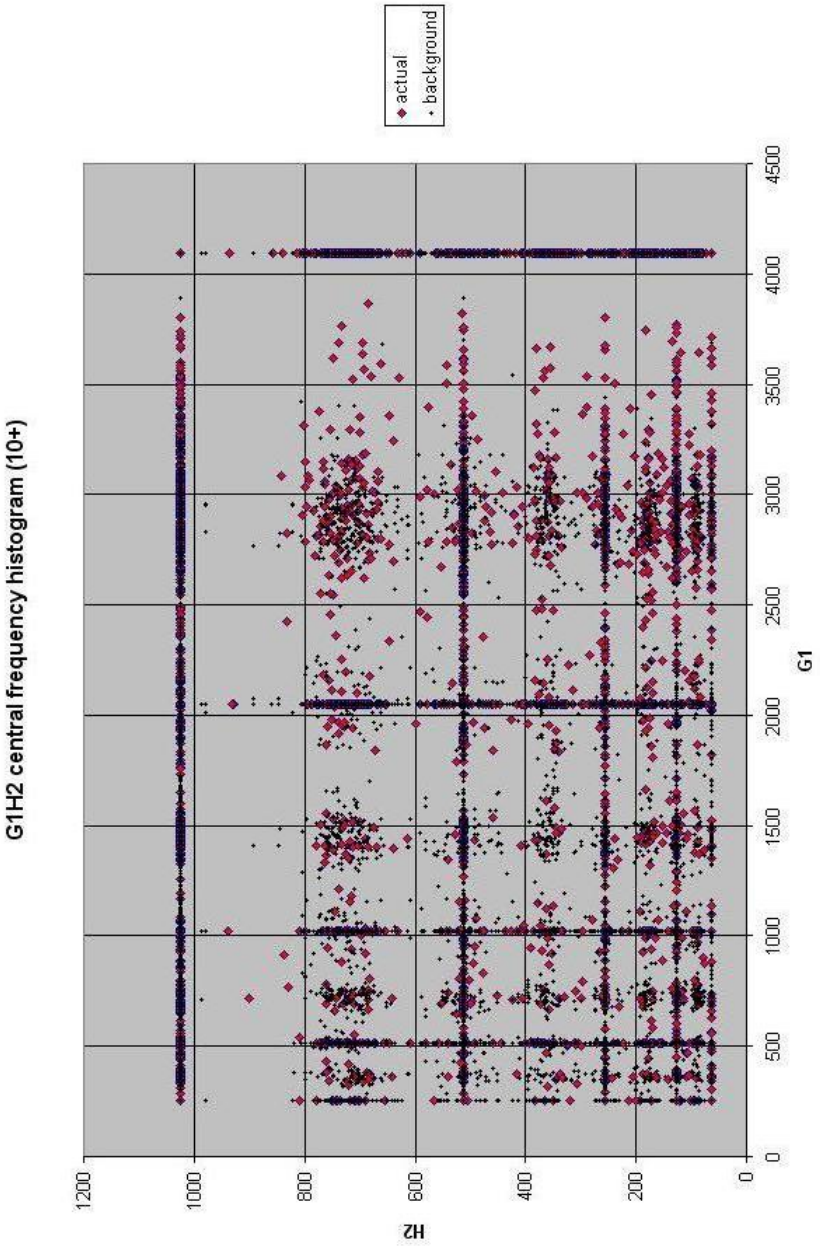


Figure 6.7: Central frequencies of accidental and actual G1H2 coincidences louder than 10

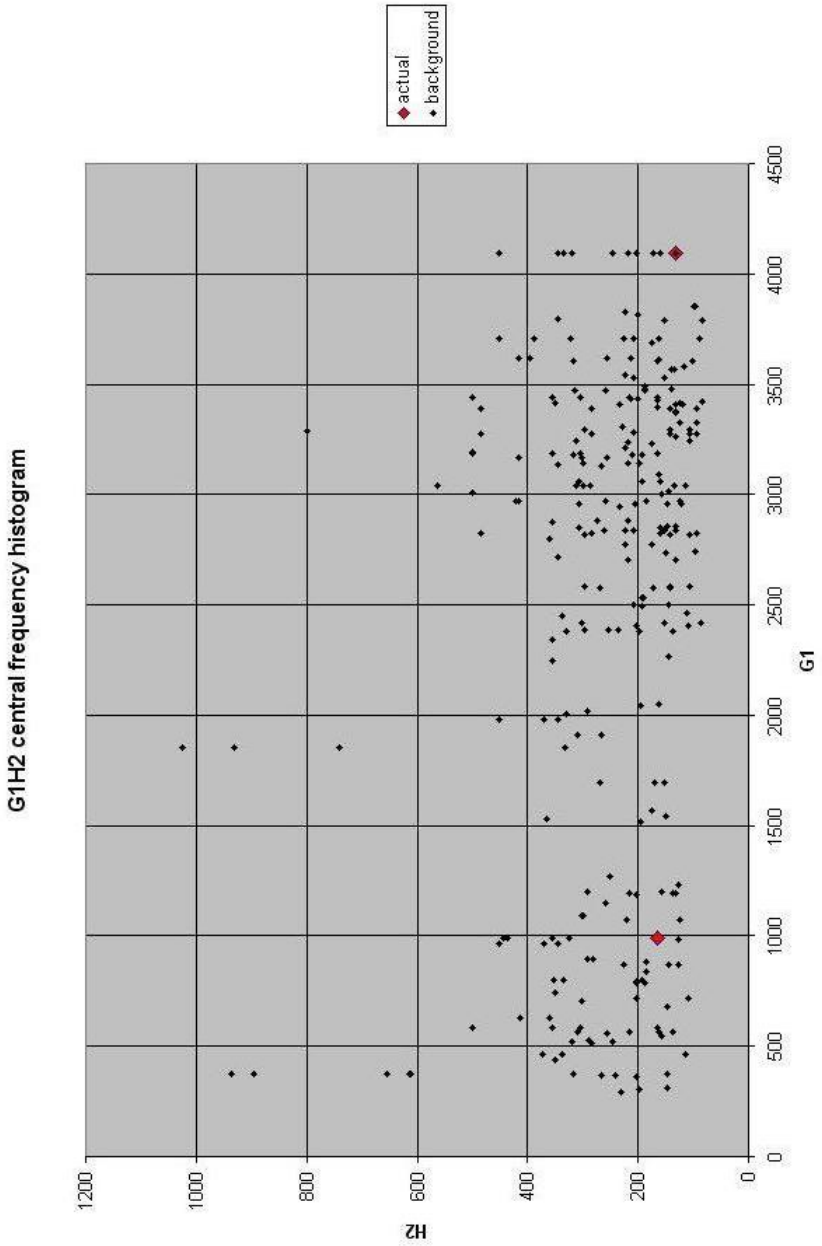


Figure 6.8: Central frequencies of accidental and actual G1H2 coincidences louder than 35

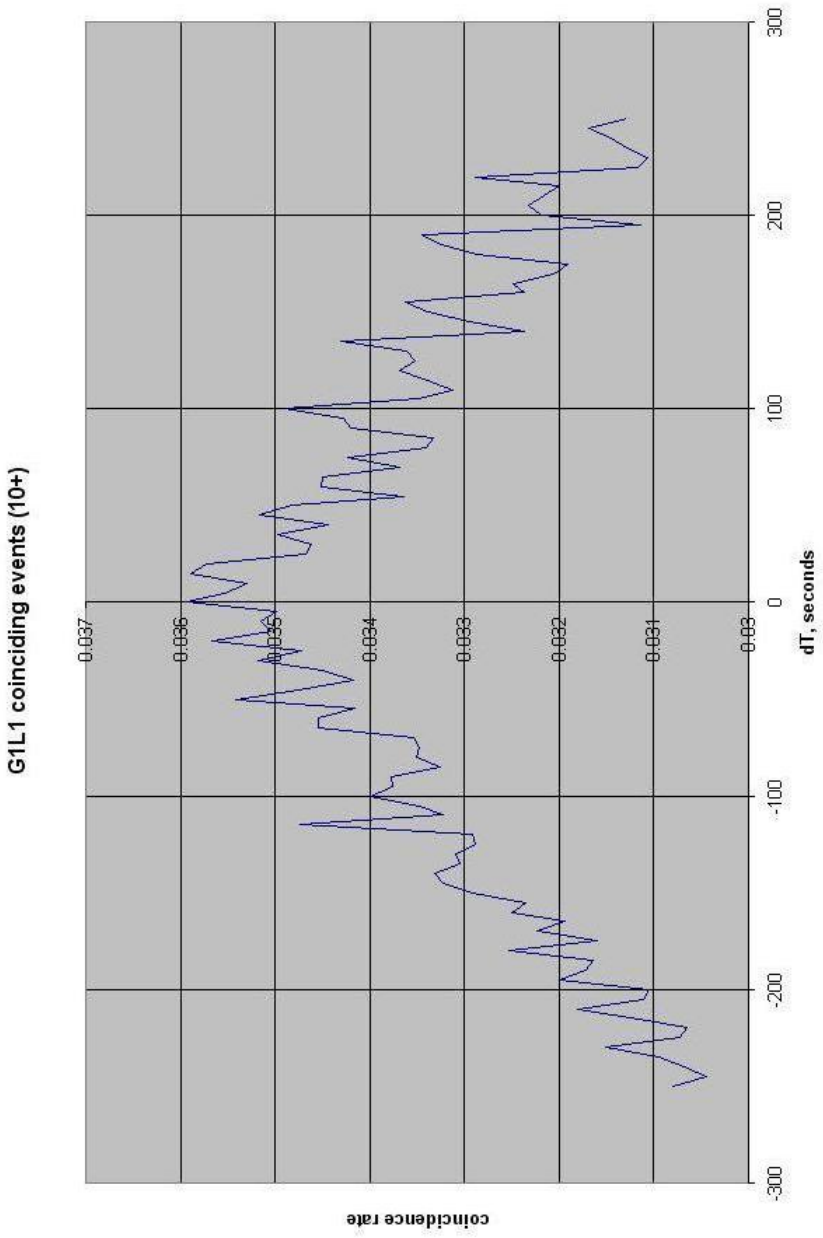


Figure 6.9: Rate of G1L1 coincidences louder than 10 vs. time shift

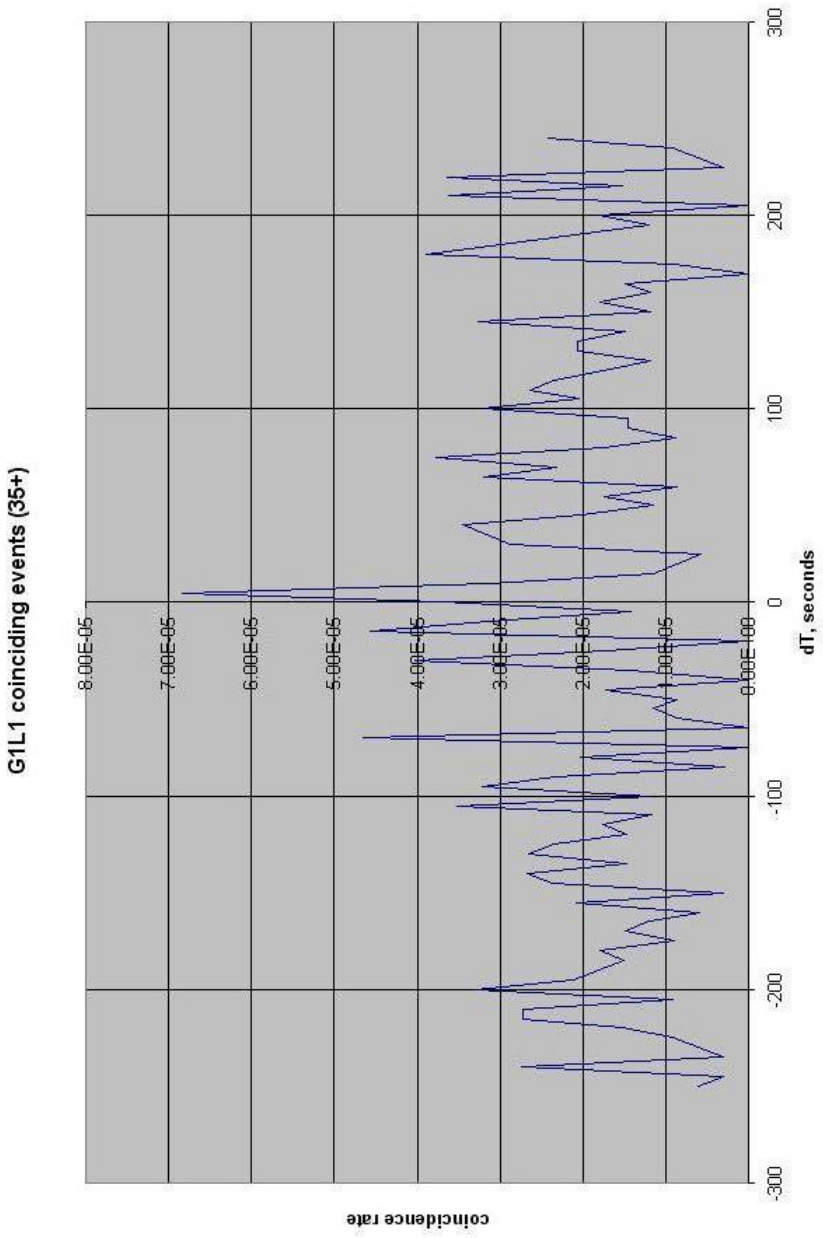


Figure 6.10: Rate of G1L1 coincidences louder than 35 vs. time shift

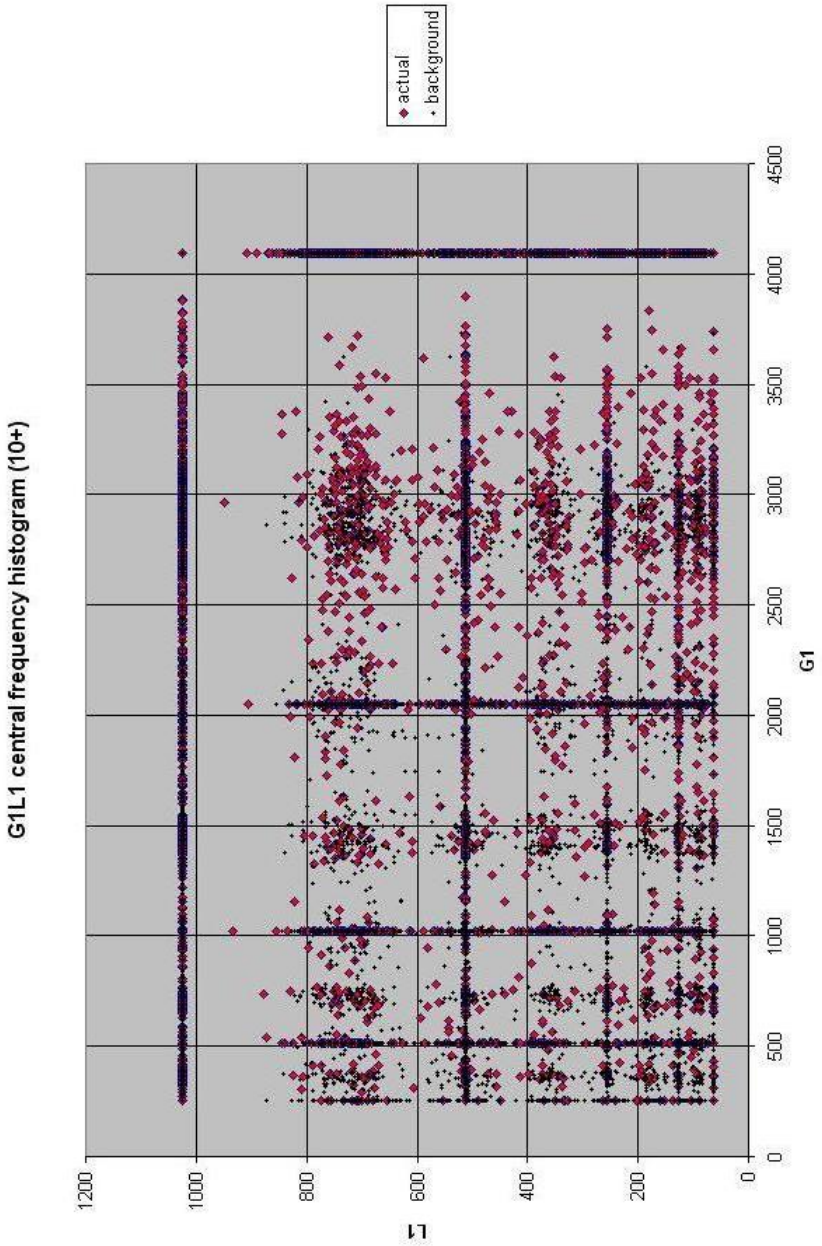


Figure 6.11: Central frequencies of accidental and actual G1L1 coincidences louder than 10

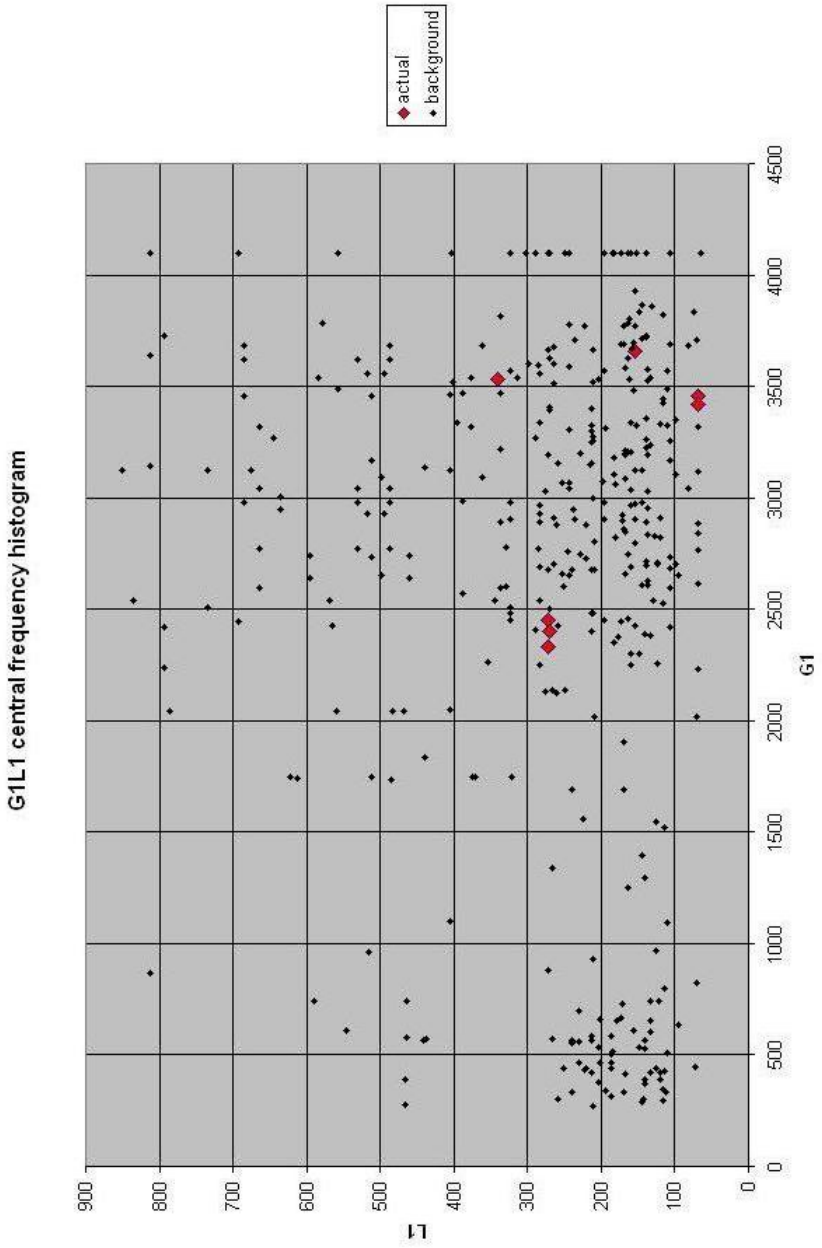


Figure 6.12: Central frequencies of accidental and actual G1L1 coincidences louder than 35

| | background coincidence rate, Hz | actual coincidence rate, Hz |
|---|---|---|
| G1H1 | 0.0293292 | .027872 |
| G1H2 | 0.0165701 | .0155821 |
| G1L1 | 0.0179185 | .0169331 |

Table 6.3: Background (accidental) and actual (non time-shifted) coincidence rates for G1H1, G1H2, and G1L1 for clustered events with significance 10 and louder

| | background coincidence rate, Hz | actual coincidence rate, Hz |
|---|---|---|
| G1H1 | 3.29264e-05 | 2.68741e-05 |
| G1H2 | 6.38538e-06 | 6.82272e-06 |
| G1L1 | 1.42301e-05 | 9.2365e-06 |

Table 6.4: Background (accidental) and actual (non time-shifted) coincidence rates for G1H1, G1H2, and G1L1 for clustered events with significance 35 and louder

## 6.2 Coincidence Analysis for Clustered Events

A separate analysis for clustered events was performed. Single coinciding events that overlapped within a window of 0.5 sec were merged[2] and files similar to those generated for single events were produced.

The coincidence rates for two significance thresholds (10 and 35) are summarized in Tables 6.3 and 6.4. A coincidence window equal to 0.05 seconds was used.

[2]In order to obtain better precision, events were merged into clusters *after* coincidences were found for *nonclustered* original triggers

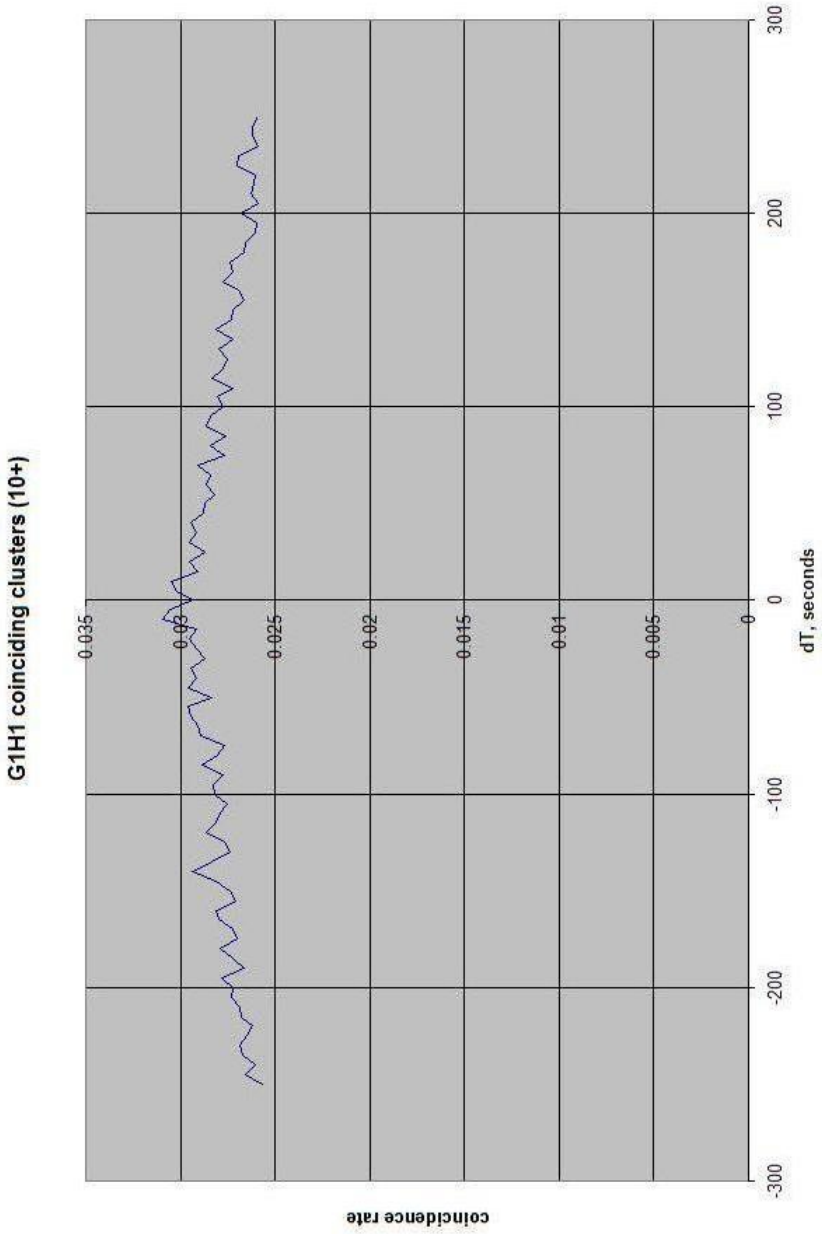


Figure 6.13: Rate of clustered G1H1 coincidences louder than 10 vs. time shift

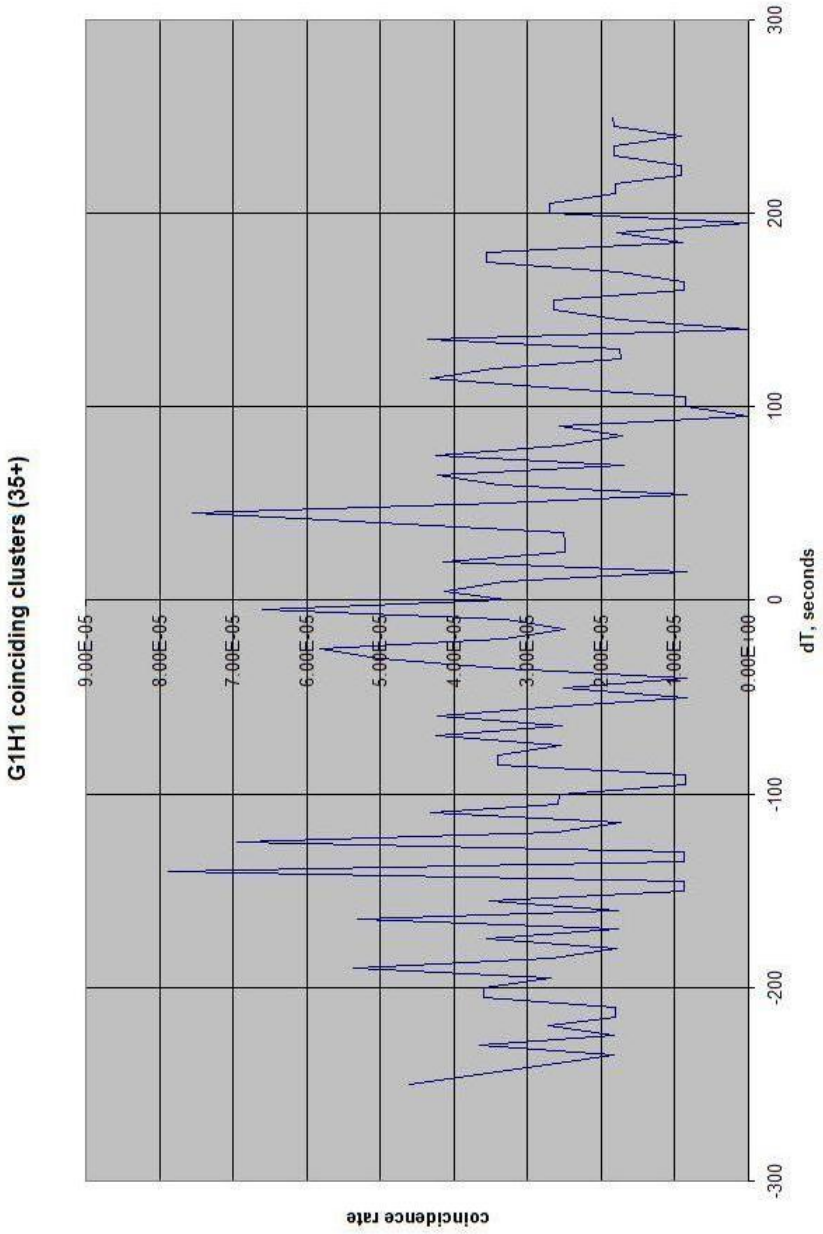


Figure 6.14: Rate of clustered G1H1 coincidences louder than 35 vs. time shift

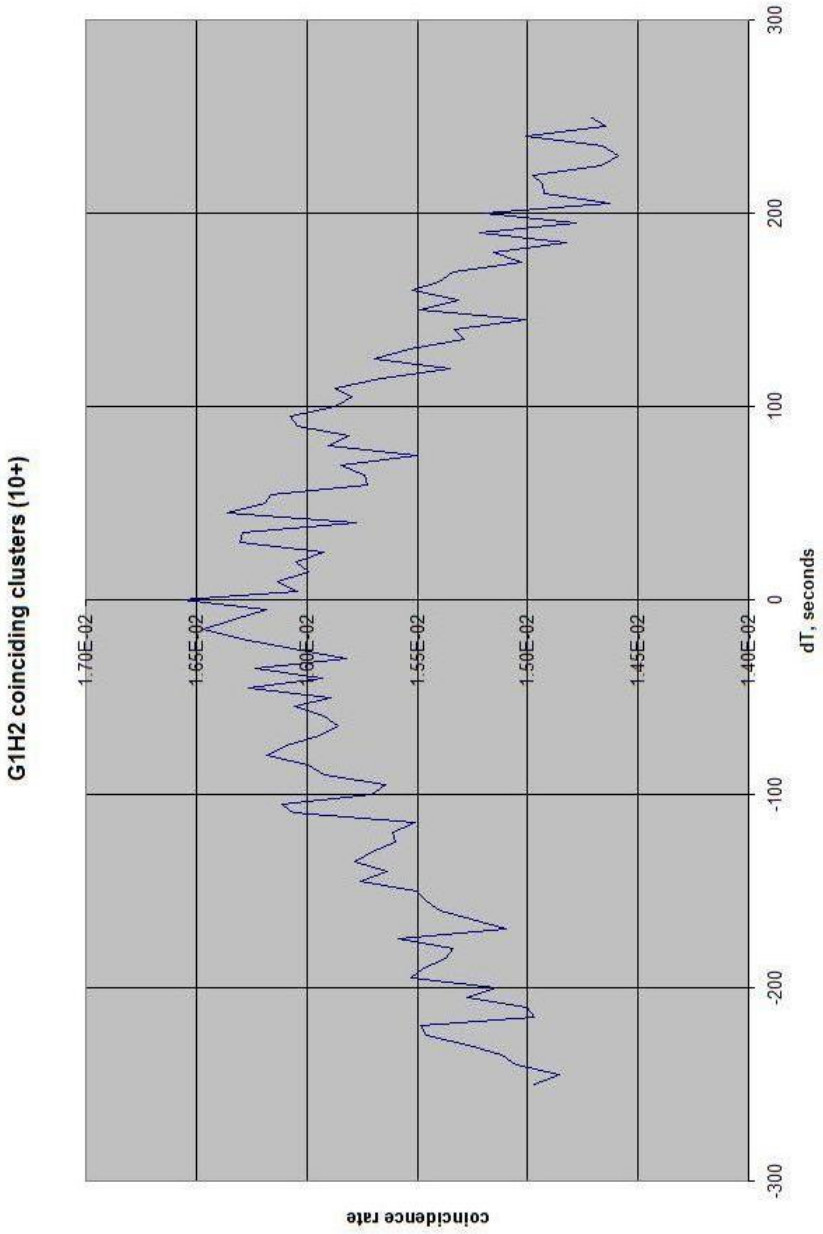


Figure 6.15: Rate of clustered G1H2 coincidences louder than 10 vs. time shift

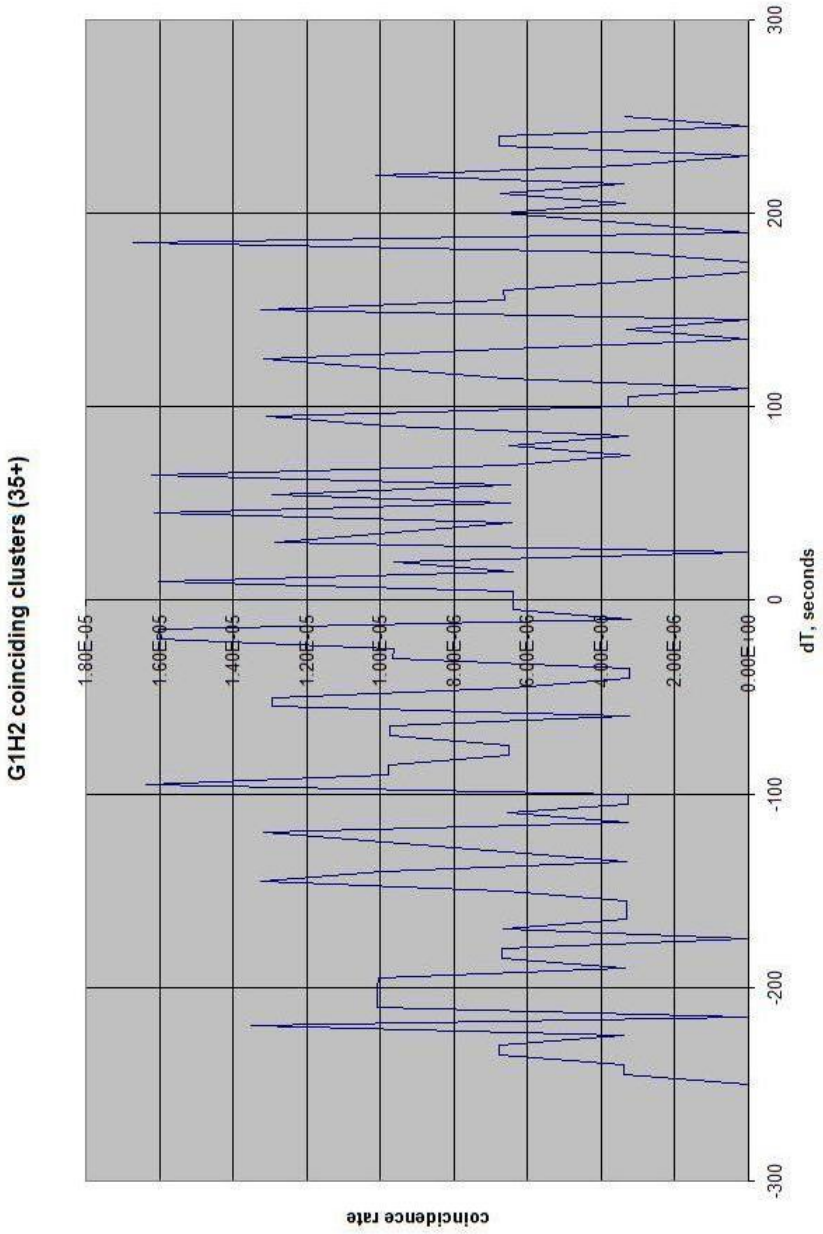


Figure 6.16: Rate of clustered G1H2 coincidences louder than 35 vs. time shift

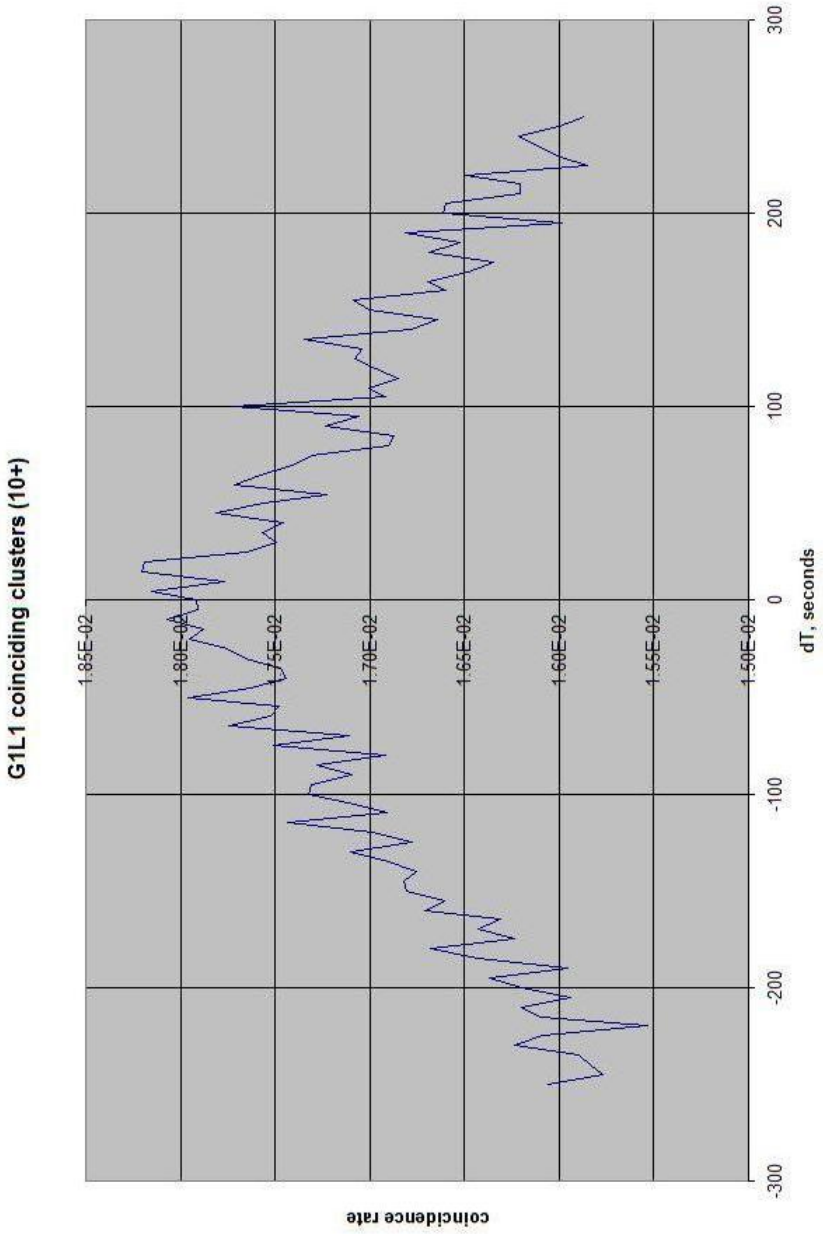


Figure 6.17: Rate of clustered G1L1 coincidences louder than 10 vs. time shift

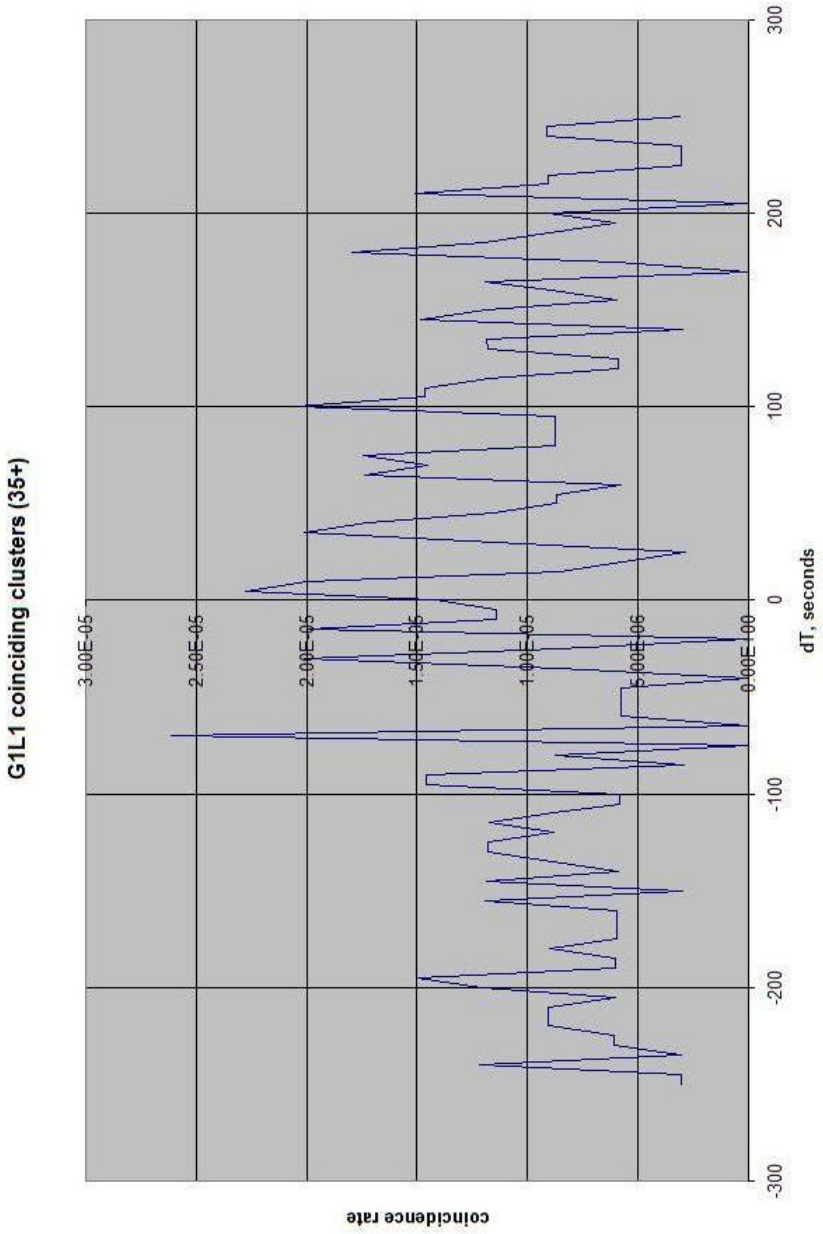


Figure 6.18: Rate of clustered G1L1 coincidences louder than 35 vs. time shift

## 6.3 Gravitational wave event candidates

Eleven loudest candidate events (that is, coincidences for which the significance of each of the two coinciding events was over 35) were identified and the characterization of these zero-lag events is currently in progress.

# Chapter 7

# Conclusions

The objective of the project was to search the double coincidence data obtained by GEO600 and the three LIGO interferometers for the gravitational wave bursts from transient astrophysical sources. The data was collected in the first year of S5 science run, which started in November 2005, and analyzed by the wavelet-based KleineWelle algorithm.

Coincidence rates for both single and clustered (within the clustering window equal to 0.5 sec) events with significance over 10 and 35 were obtained. In order to take into account the time a gravitational wave would take to get from GEO600 to the LIGO detectors, as well as experimental uncertainty due to response of the instruments and the search methods used, the coincidence window was set to 0.05 sec. Background coincidence rates were also obtained by time shifting the time series from one detector with respect to that of the other.

Eleven candidate events with significance over 35 were identified, with their characterization currently in progress.

# Bibliography


[1] http://en.wikipedia.org/wiki/Hulse-Taylor_binary.

[2] Lindy Blackburn. Kleinewelle technical document.

[3] Shourov Chatterji. *The search for gravitational-wave bursts in data from the second LIGO science run*. PhD thesis, MIT, 2005.

[4] Nelson Christensen. Veto studies for ligo inspiral triggers. *Class. Quantum Gravity*, 22, 2005.

[5] P. C. W. Davies. *The Search for Gravity Waves*. Cambridge University Press, 1980.

[6] Harvey Gould and Jan Tobochnik. Thermal and statistical physics. will be published by Princeton University Press in 2009.

[7] Keith Riles. http://gallatin.physics.lsa.umich.edu/ keithr/S5DQ/flaginfo.html.

[8] Bernard F. Schutz. *A first course in general relativity*. Cambridge University Press, 1985.